Int. J. Electrochem. Sci., 14 **(2019)** 1093 – 1106, doi: 10.20964/2019.02.48

International Journal of
ELECTROCHEMICAL
SCIENCE
www.electrochemsci.org

Catalytic Activity of Ni-YSZ composite as Anode for Methane Oxidation in Solid Oxide Fuel Cells

Yanting Tian[1,*], *Zhe Lü*[2,*], *Xiang Guo*[1], *Pingping Wu*[1]

[1] College of Physics and Optoelectronics, Taiyuan University of Technology, Taiyuan 030024, China
[2] Department of Physics, Harbin Institute of Technology, Harbin 150001, China
[*]E-mail: yanting_005@163.com, lvzhe@hit.edu.cn

Received: 4 September 2018 / *Accepted:* 12 November 2018 / *Published:* 5 January 2019

Natural gas has been exploited as an available energy source for solid oxide fuel cells in recent years. However, the problem of carbon deposition that forms on nickel-based anodes by using direct methane results in performance failure of cells. It is well known that the catalytic partial oxidation of methane is a good solution to suppress carbon formation. Herein, we present an investigation of the catalytic activity of Ni/YSZ cermet anodes as a function of the CH_4/O_2 flow rate ratio ($1 \leq R_{in} \leq 5$). The behavior of methane catalytic activity was characterized using mass spectrometry (MS) and temperature-programmed oxidation (TPO). The catalytic activity of methane oxidation at 700 °C showed that Ni oxidation occurred at $R_{in} \leq 1.67$. A basic equilibrium to prevent carbon deposition and Ni oxidation occurred at $R_{in} = 2.5$, which exhibited the best activity among the Ni/YSZ electrodes. Through the electrochemical measurements and impedance spectroscopy analysis of the cell, it was proved that the cell possessed the lowest ohmic resistance and optimized output performance at $R_{in} = 2.5$. In addition, a stable cell operation at 0.9 V was guaranteed without serious degradation.

Keywords: Solid Oxide Fuel Cells, Catalytic Activity, CH_4/O_2 Ratio, Ni-YSZ Anode, Partial Oxidation

1. INTRODUCTION

Solid oxide fuel cells (SOFCs) have attracted particular attention recently due to their environmental friendliness, high energy conversion efficiency and fuel flexibility [1]. In addition to hydrogen, hydrocarbon fuels, carbon monoxide, and solid carbon can all be used as potential fuels for SOFCs [2]. Hydrocarbon fuels are more widely available and are more safely stored and transported than hydrogen. Additionally, using hydrocarbon as fuel can further reduce the cell operating cost by eliminating the external reforming process. Specifically, methane (CH_4), which has an abundant and reliable long-term supply, is one of the most attractive fuels for SOFCs [3-5].

As the commonly used anode material in SOFCs, Ni-based cermet has excellent electrical conductivity and good catalytic properties for fuel oxidation. However, hydrocarbon fuels can form carbon deposits on Ni catalysts, which are deposited in the internal pores of the anode and block the fuel diffusion into the porous electrode. As a result, the gas diffusion resistance of the cell is increased and the electrochemical catalytic activity of the Ni-based cermet is deactivated [6-8]. Significant efforts have been spent on preventing carbon formation over Ni-based anodes. When methane is adopted as the fuel for SOFCs, it is typically reformed to H_2 and CO by indirect reforming processes, such as steam reforming, dry reforming and catalytic partial oxidation (CPOX) [9-11]. The addition of oxygen-containing gases into the anodic feeding gas mixture could increase the O/C ratio and therefore thermodynamically avoid carbon formation [12]. In this sense, the catalytic partial oxidation of CH_4 over the Ni catalyst could be a better cost- and energy-efficient way to restrain carbon formation and obtain a high CH_4 conversion efficiency.

Existing studies have showed the potential superiority of adding air to the anodic feeding gas mixture. Pillai et al. [13] reported that the stability of the cell performance could be increased by using air as an additive to methane. Aslannejad et al. [14] explored the impact of the addition of air to methane for the Ni/YSZ anode supported SOFCs. The optimal gas component of a 1:5 air to methane addition was determined. Through impedance spectroscopy analysis and voltage measurements, it was proved that both carbon deposition and anode delamination were avoided under this condition. Lee et al. [15] demonstrated that robust CPOX-based SOFCs fueled by CH_4 could restrain carbon deposition and Ni oxidation. Adding oxygen to methane could fundamentally prevent carbon deposition, while Ni oxidation was prevented by (electro)catalytic reaction controls and oxygen ionic conductors. To date, however, few studies have truly investigated the subject of the catalytic partial oxidation approach with O_2 added to methane on the performance of SOFC anodes since the partial O_2 pressure in the gas chamber should be maintained below 10-18 atm to achieve an electrochemical potential gradient of the SOFC [15]. In addition, an excessive O_2 content in the anode gas chamber may result in Ni oxidation [16-17].

In the present work, we focused on the study of the catalytic activity of Ni/YSZ electrodes as a function of the incoming CH_4/O_2 flow rate ratio (R_{in}). The behavior of methane catalytic oxidation was characterized by mass spectrometry (MS) as a function of the consumption of methane and the resulting yields of H_2, CO and CO_2. The carbon deposition and Ni oxidation were investigated. The electrochemical performances and impedance spectroscopy analysis of the single cell were also tested under various CH_4/O_2 gas flow rates.

2. EXPERIMENTAL

2.1 Catalyst preparation

NiO (Inco, Canada), YSZ (TZ-8Y, Tosoh Corp. Japan) and tapioca starch powders were mixed at a weight ratio of 5:5:2, thereby forming the anode catalysts, which were pressed into disk shaped pellets 13 mm in diameter. The as-prepared catalyst disks were calcined at 1000 °C for 2 h to remove the volatile phases, which were followed by sintering at 1400 °C for 4 h in air. Then, the green catalysts were reduced from NiO to Ni using humidified hydrogen (H_2, 3 vol.% H_2O) at 700 °C for the catalytic

activity tests.

2.2 Catalytic activity measurements

The catalytic activity of the nickel-based samples was tested under various gas mixtures. Fig. 1 presents the schematic diagram of the experimental apparatus. The catalytic tests were performed using a fixed-bed quartz reactor (inner diameter: 8 mm). The inlet and outlet gas compositions were analyzed using an LC-D100 mass spectrometer (Ametek, America). The as-prepared Ni/YSZ catalyst samples were inserted into the middle of the quartz tube between quartz wools.

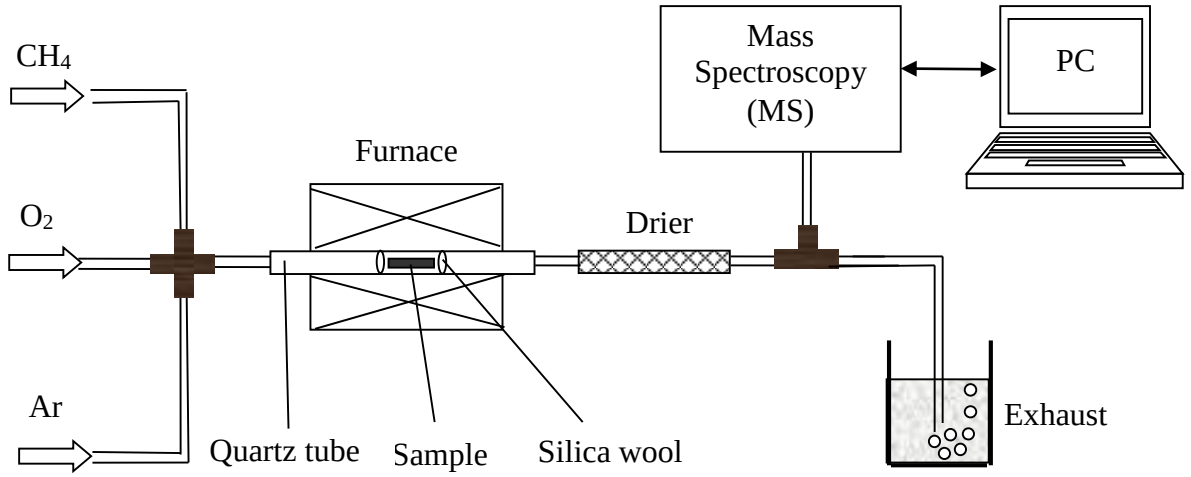

Figure 1. Schematic diagram of the experimental apparatus used for the mass spectrometer tests

The carbon depositions of the Ni/YSZ electrodes under direct methane without oxygen were measured. The samples were treated under flowing CH_4 (25 vol.% in Ar, 100 sccm) at 650 °C, 700 °C and 750 °C for 2 h. The temperature was increased from 50 °C to the testing temperatures with a linear heating rate of 8 °C/min under an Ar atmosphere. Temperature-programmed oxidation (TPO) was employed to measure the amount of carbon deposition on the Ni/YSZ anodes operating in the CH_4 atmosphere. The total feed flow rate was 100 sccm (10 vol.% O_2 in Ar) and was controlled using mass flow controllers.

Catalytic activity tests of the Ni/YSZ catalysts under CH_4/O_2 gas mixtures were conducted using temperature-programmed reactions performed in continuous-flow methane/oxygen mixtures as a function of the CH_4/O_2 flow rate ratio ($1 \leq R_{in} \leq 5$, see Table 1). The temperature was raised from room temperature to 850 °C at a heating rate of 10 °C/min. The CH_4, CO, CO_2 and H_2 evolutions were recorded as a function of the temperature. The carbon deposition behavior was characterized by temperature-programmed oxidation tests.

Table 1. The various flow compositions of the gas mixture

Gas	R_{in}	Ar (sccm)	CH_4 (sccm)	O_2 (sccm)
1	5	70	25	5
2	2.5	65	25	10
3	1.67	60	25	15
4	1.25	55	25	20
5	1	50	25	25

The catalytic oxidation of methane under various CH_4/O_2 flow rate ratios at 700 °C was tested for 5 h. The weights of the samples before and after catalytic activity measurements were recorded. The temperature-programmed oxidation tests were also employed for carbon deposition.

2.3 Fabrication and characterization of single cells

The anode-supported cells composed of Ni/YSZ anodes, YSZ electrolyte films and modified $La_{0.7}Sr_{0.3}MnO_3$ (LSM) cathodes were fabricated. The anode substrates were prepared in the same way as the NiO/YSZ catalysts calcined at 1000 °C. YSZ films were spin-coated on the anode substrates and sintered at 1400 °C for 4 h [18]. The LSM cathodes were pasted on the YSZ films with a size of 0.14 cm^2, which were followed by impregnating in the $Sm_{0.2}Ce_{0.8}(NO_3)_x$ (SDC) solution [19]. The anode substrates were reduced in hydrogen at 700 °C before electrochemical performance tests.

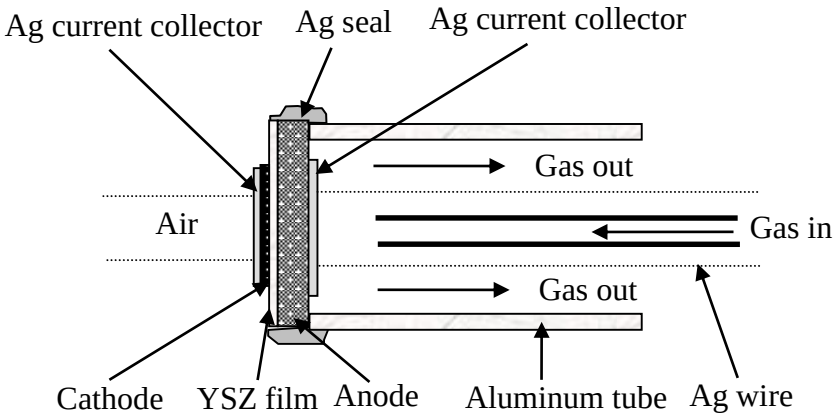

Figure 2. Schematic diagram of the cell testing arrangement

Silver paste (DAD-87, Shanghai Research Institute of Synthetic Resin, China) was used to fix and seal the fuel cell to an aluminum tube. The schematic diagram of the cell testing arrangement was shown in Fig. 2. The fuel cell was tested by the four-probe method in a furnace at 700 °C. The methane/oxygen mixtures and ambient air were used as the fuel and oxidant, respectively. The cell performances and electrochemical impedance spectra were measured by a BiStat potentiostat (Bio-logic SAS, France). The frequency ranged from 91 kHz to 0.1 Hz with a signal amplitude of 10 mV.

3. RESULTS AND DISCUSSION

3.1 Catalytic activity of Ni/YSZ catalysts under methane fuel

The amount of carbon deposited on the anode catalyst was dependent on the evolved carbon dioxide, which was monitored by the TPO testing. Fig. 3a shows the TPO profiles of the Ni/YSZ catalysts after being in a 25% CH_4-75% Ar gas mixture at different testing temperatures for 2 h. As can be seen, the carbon dioxide peaks were found in the temperature range from 450 to 700 °C when the catalyst was programmed at 700 °C.

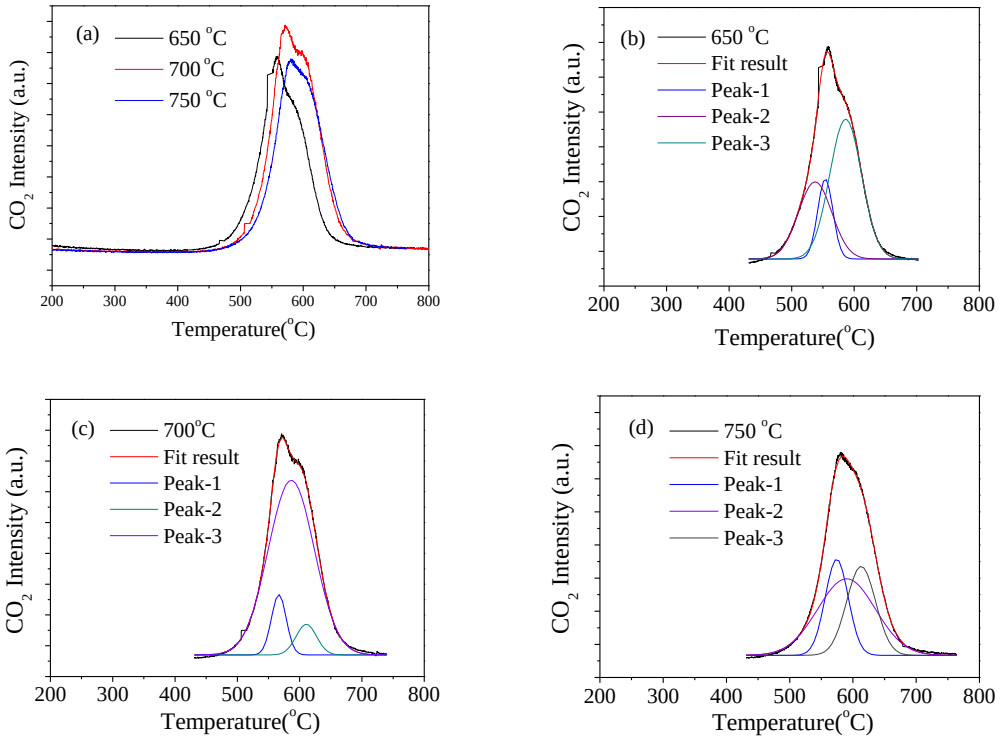

Figure 3. (a) TPO profiles of the Ni/YSZ catalyst operated at different temperatures, (b-d) The fitting results of the TPO profiles programmed at 650 °C, 700 °C and 750 °C

The TPO curves of the Ni/YSZ catalyst programmed at 750 °C possessed the same temperature range to remove the carbon deposits. However, the lower carbon dioxide peaks of 750 °C indicated a lower carbon deposit amount. The temperature to remove the carbon deposits was significantly reduced when the catalyst was programmed at 650 °C, and the carbon dioxide peaks were also lower than that programmed at 700 °C. The reactive performance of carbon oxidation could be obtained by the TPO curves. The temperature at which the carbon dioxide peak had a maximum value depended on the reactivity of the deposit; the higher the peak temperature was, the lower the carbon reactivity toward oxidation was [20]. These results indicated that the deposit had higher reactivity and the amount of deposited carbon was decreased when the Ni/YSZ catalysts were programmed at 650 °C.

The fitting results of each TPO profile are shown in Figs. 3b-3d. It is found that the carbon dioxide peaks of each TPO profile can be divided into three peaks, and the temperatures at which the

peaks have a maximum value and the area proportions of each fitting peak are shown in Table 2. The temperature values of the carbon dioxide peaks tested at 650 °C were 537, 555 and 587 °C, and the peak at 587 °C had the highest proportion of 53.8%. The temperature values of the fitting peaks tested at 700 °C and 750 °C were essentially the same. The highest proportions of 700 °C and 750 °C were both obtained at the peak of 588 °C, the same as that tested at 650 °C. By comparing the areas under the fitting curves, it was found that the TPO profile tested at 700 °C had the largest area, which had the highest amount of deposited carbon. Caine et al. [21] tested Ni/ZrO_2 anodes in a dry methane/helium gas mixture from room temperature to 900 °C. They found that the rate of methane adsorption over the Ni/ZrO_2 anodes had a maximum value at 700 °C, which was consistent with our results.

Table 2. Fitting results of the TPO tests

Testing temperature (°C)	Temperature value of each fitting peak (°C)	Area of each fitting peak	Proportion of each fitting peak	Area of the fitting result
650	537	7.16×10^{-7}	30%	2.36×10^{-6}
	555	3.48×10^{-7}	14.7%	
	587	12.7×10^{-7}	53.8%	
700	567	2.9×10^{-7}	9%	3.13×10^{-6}
	588	2.6×10^{-6}	83%	
	609	2.04×10^{-7}	65%	
750	572	6.57×10^{-7}	23.8%	2.76×10^{-6}
	588	1.33×10^{-6}	48.2%	
	611	7.64×10^{-7}	27.7%	

3.2 Catalytic activity of Ni/YSZ catalysts under CH_4/O_2 gas mixtures

Fig. 4 presents the influence of the CH_4/O_2 flow rate ratio ($1 \le R_{in} \le 5$) on the catalytic activity of Ni/YSZ catalysts with various temperatures. The components of the incoming gas mixtures are given in Table 1. The MS signals of the exit gas species (CH_4, H_2, CO and CO_2) during the catalytic testing were analyzed as a function of R_{in}. It can be seen that the dissociative methane adsorption occurred at temperatures above 490 °C. The methane conversion rate was found to be increased with the increasing temperature, while the yields of H_2 and CO were increased correspondingly. Although the catalytic oxidation reactions involve a complex series of reaction mechanisms, some chemical reactions could possibly exist in the partial oxidation of methane (Eqs. (1)-(4)) [22-23]:

$$CH_4 + \frac{1}{2}O_2 \rightarrow CO + 2H_2 \quad (1)$$

$$CH_4 + O_2 \rightarrow CO + H_2 + H_2O \quad (2)$$

$$CH_4 + O_2 \rightarrow CO_2 + 2H_2 \quad (3)$$

$$CH_4 + \frac{3}{2}O_2 \rightarrow CO + 2H_2O \quad (4)$$

and, of course, complete oxidation (Eq. (5))

$$CH_4 + 2O_2 \rightarrow CO_2 + 2H_2O \quad (5)$$

Steam reforming (Eq. (6)) and CO_2 reforming (Eq. (7)) may generate syngas [23]:

$$CH_4 + H_2O \rightarrow CO + 3H_2 \quad (6)$$

$$CH_4 + CO_2 \rightarrow 2CO + 2H_2 \quad (7)$$

As shown in Fig. 4d, the intensity of CO_2 was decreased with temperature, which indicated that CO_2 was consumed by the reforming reaction of Eq. (7). In addition, the generated H_2 and CO could also be oxidized by Eqs. (8)-(9):

$$H_2 + O_2 \rightarrow H_2O \quad (8)$$

$$CO + \frac{1}{2}O_2 \rightarrow CO_2 \quad (9)$$

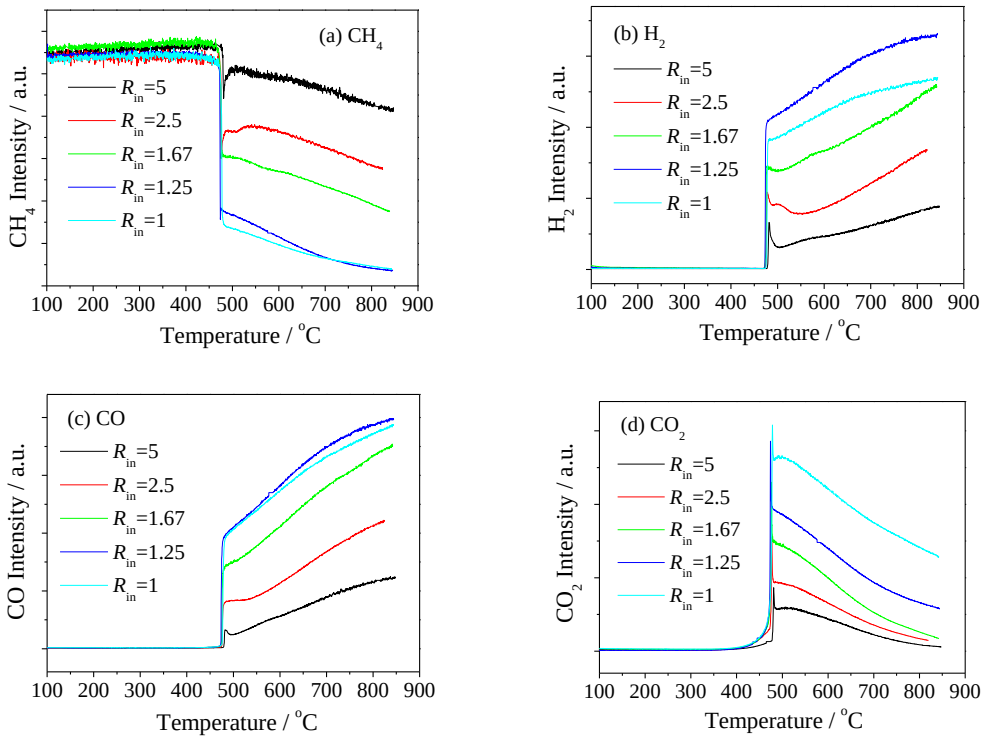

Figure 4. Catalytic activity of Ni/YSZ catalysts in CH_4/O_2 mixtures with varying temperatures: (a) CH_4, (b) H_2, (c) CO and (d) CO_2

The conversion of methane was increased gradually with the increasing oxygen content. The yields of H_2 and CO were also increased with the increasing oxygen content. However, the intensities of H_2 and CO at $R_{in} = 1$ were less than those at $R_{in} = 1.25$, while the amount of CO_2 generated at $R_{in} = 1$ was obviously higher than that at $R_{in} = 1.25$. These results indicated that the reaction rate of complete oxidation (Eq. (5)) was higher than that of partial oxidation at $R_{in} = 1$. The complete oxidation reaction of methane (Eq. (5)) was the dominant reaction at $R_{in} = 1$, and the reaction at $R_{in} \geq 1.25$ was dominated by the partial oxidation of methane. The TPO profiles of the Ni/YSZ catalysts after being in various methane/oxygen mixtures are shown in Fig. 5. The amount of CO_2 detected by TPO was found to

decrease with the increasing oxygen content in the gas mixture, which indicated that the deposited carbon decreased gradually. When the flow rates of O_2 in the mixture were 10 and 15 sccm (R_{in} = 2.5 and 1.67), the temperature range of the TPO was between 430 to 670 °C and the peak value appeared at 560 °C. When the O_2 flow rates were increased to 20 and 25 sccm (R_{in} = 1.25 and 1), the peak value was reduced to 530 °C. With the increasing oxygen content, the temperature to eliminate the deposited carbon decreased, which indicated that the elimination of the deposits became easier. The effect of oxygen on the reforming reactions of methane is favorable to inhibit the carbon deposition on the Ni/YSZ anode.

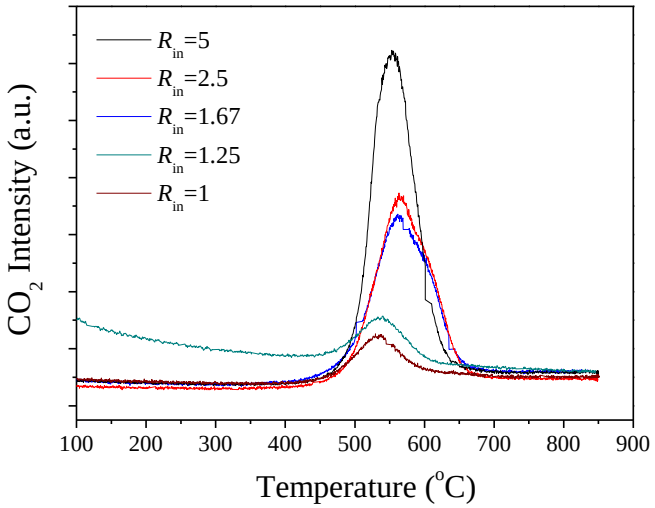

Figure 5. TPO profiles of Ni/YSZ catalysts after being in various methane/oxygen mixtures

Table 3. Carbon deposition of the anode under various CH_4/O_2 ratios at 700 °C for 5 h

O_2 flow rate (sccm)	R_{in}	m_1 (mg)	m_2 (mg)	weight increase rate (%)	Carbon deposition rate (mg/h)
0	-	113.12	117.02	3.45	0.78
5	5	117.97	118.12	0.13	0.03
10	2.5	109.56	109.75	0.17	0.038
15	1.67	108.67	109.97	1.3	-
20	1.25	113.89	114.08	1.67	-
25	1	110.81	111.04	1.98	-

The catalytic activity of Ni/YSZ catalysts was tested under various CH_4/O_2 ratios at 700 °C for 5 h. The weights of the catalysts before and after catalytic activity tests were measured for carbon deposition. As shown in Table 3, m_1 and m_2 represent the quality of the catalysts before and after the catalytic activity tests, respectively. It was found that the catalyst that was exposed to the methane atmosphere without oxygen for 5 h (CH_4 25 sccm-Ar 75 sccm) had the highest weight increase rate of 3.45%, and the carbon deposition rate was 0.78 mg/h. When methane was mixed with 5 sccm and 10 sccm oxygen, the weight increase rate decreased to 0.13% and 0.17%, respectively. With the oxygen flow rate continued to increase, the weight increase rate of the catalysts increased gradually. The greater

the oxygen content, the higher the weight increase rate.

The TPO profiles of the deposited carbon after reforming reactions at 700 °C are shown in Fig. 6a. When the Ni/YSZ catalyst was exposed to a methane atmosphere without oxygen, the temperature range was between 450 to 700 °C and the peak value appeared at 567 °C. When methane was loaded with 5 sccm oxygen, the carbon dioxide peak was significantly decreased.

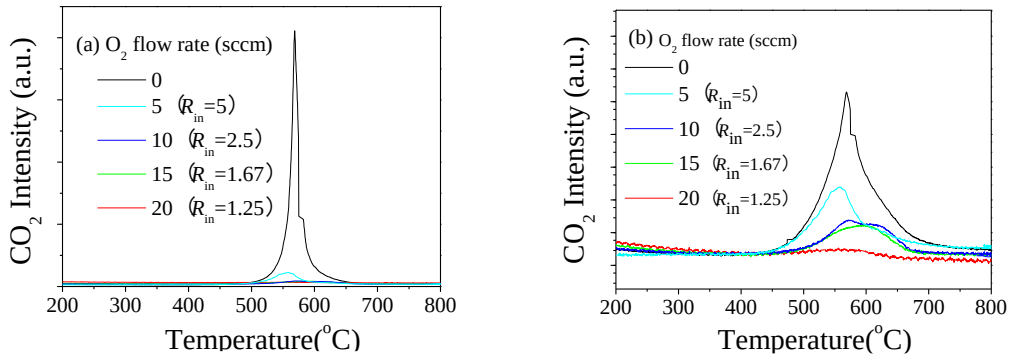

Figure 6. TPO profiles of Ni/YSZ after being exposed to various CH_4/O_2 gas mixtures at 700 °C for 5h: (a) initial data and (b) using the Log function on the ordinate axis

This result indicated that the addition of O_2 inhibited the carbon deposits in the anode. As the amount of oxygen content continued to increase, CO_2 was hardly detected in the TPO profiles. Therefore, the vertical axis was processed using the logarithm, as shown in Fig. 6b. The amounts of deposited carbon at R_{in} = 2.5 and R_{in} = 1.67 were basically the same. A weak peak of CO_2 was observed at R_{in} = 1.25, indicating that the carbon accumulation was extremely small. It can be explained from the TPO results that the increased weight of the catalyst at $R_{in} \leq 1.67$ given in Table 3 was not due to carbon deposition, but rather due to the oxidation of the metal Ni at the anode (Eq. (10)) with excessive oxygen content [24-25] :

$$2Ni + O_2 \rightarrow 2NiO \qquad (10)$$

The CH_4/O_2 mixture is an important determinant of the coexistence of two phases of Ni and NiO [24]. The ratio of CH_4/O_2 controls the content of Ni and NiO in the anode. Excessive amounts of O_2 lead to the formation of NiO, thus resulting in the loss of catalytic activity of the anode. Furthermore, the excessive O_2 content also increases the direct oxidation of the fuel, thereby resulting in an increase in the production of CO_2 and a reduction in the fuel utilization. The results given by table 3 and the TPO tests indicated that Ni oxidation occurred at $R_{in} \leq 1.67$. Meanwhile, R_{in} = 2.5 was an equilibrium since both carbon deposition and Ni oxidation were not obvious, which was an optimal gas proportion.

3.3 Electrochemical performance of single cells

flow rates were fixed at 50 sccm. The open-circuit voltage (OCV) reached 1.09 V at the oxygen flow rate of 10 sccm. When the oxygen flow rate increased from 30 sccm to 40 sccm, the OCV decreased significantly from 1.07 V to 1.02 V, as shown in Table 4. A decrease of the OCV occurred with the

increasing oxygen content. The increase of the partial oxygen pressure on the anode led to the decrease of the local oxygen concentration gradient between the cathode and anode, and resulted in a decrease of the OCV. When the flow rate of oxygen reached 50 sccm, the OCV was reduced to below 1 V. The maximum power densities (MPDs) were 428, 467 and 497 mW/cm^2 at R_{in} = 5, 2.5 and 1.67, respectively. However, the concentration polarization phenomenon appeared under high current of the discharge curve at R_{in} = 1.67. According to the analysis in section 3.2, the reaction at R_{in} = 1.67 was dominated by the partial oxidation of methane. It seemed that electrochemical complete oxidation of methane (Eq. (11)) existed under high current, which caused the concentration polarization phenomenon due to the formation of H_2O and CO_2.

$$CH_4 + 4O^{2-} \rightarrow CO_2 + 2H_2O + 8e^- \quad (11)$$

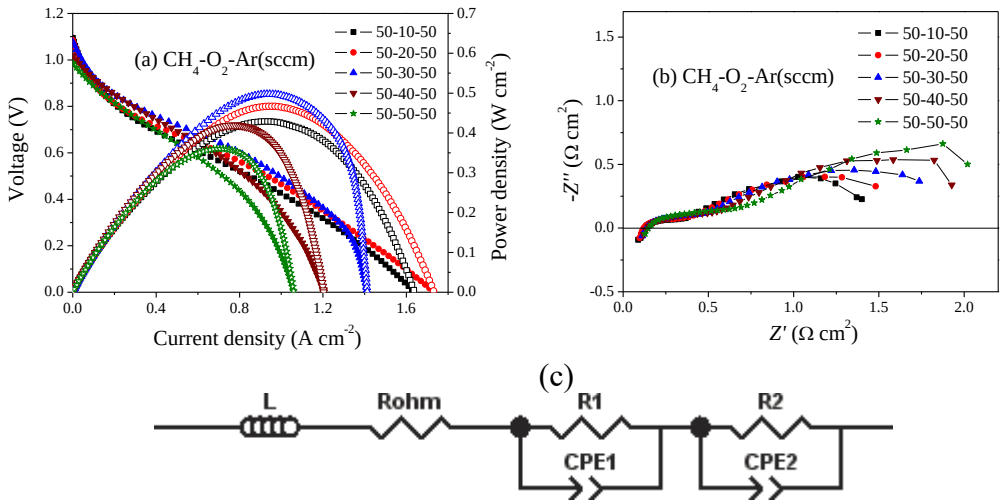

Figure 7. (a) Output performance of the cell under CH_4/O_2 gas mixtures, (b) Impedance spectra of the single cells under open-circuit conditions, and (c) The equivalent circuit of the impedance spectra

By continuing to increase the oxygen content to 40 and 50 sccm (R_{in} = 1.25 and 1), the concentration polarization phenomenon under high currents become more obvious. This is because with the increased oxygen concentration, more non-electrochemical active products (CO_2 and H_2O) are generated from the complete oxidation reaction, which are deleterious to the electrochemical oxidations of H_2 and CO. The concentration overpotential under high current seriously limits the output performance of the cell. In addition, with the oxygen surface concentration increased, the NiO formed by the reaction of oxygen atoms with Ni metal resulted in an interruption of the anode current pathway and a lower cell performance. The maximum power densities were significantly reduced to 419 and 360 mW/cm^2 at R_{in} = 1.25 and 1, respectively. The *I-V* and *I-P* curves confirmed that R_{in} = 2.5 was appropriate for the cell performance.

The AC impedance spectra of the cells measured under the open circuit voltage condition are shown in Fig. 7b. These spectra were fitted using an equivalent circuit in Fig. 7c with two semicircles, $LR_{ohm}(R_1CPE_1)(R_2CPE_2)$. In this circuit, L is the inductance, which is mainly attributed to silver voltage-current probes; R_{ohm} is the ohmic resistance, including the electrolyte resistance, contact resistances, and

electrode ohmic resistance; and (R_1CPE_1) and (R_2CPE_2) correspond to the high- and low-frequency arcs, respectively. The high frequency resistance R_1 is attributed to the charge-transfer polarization, while the low frequency resistance R_2 is mainly due to the gas dissociative adsorption and/or surface diffusion resistance [26]. The ohmic resistance is determined by the actual temperature of the cell [27]. From the fitting results of the impedance spectra in Table 4, the cell tested at R_{in} = 2.5 had the lowest ohmic resistance of 0.120 Ω·cm^2, which presented direct evidence of a higher temperature. When continuing to increase the oxygen content, the ohmic resistance increased obviously. The temperature dropped due to the inferior catalytic effectiveness of NiO for exothermic reactions. It can be seen from the impedance spectra that the low frequency semicircle of the gas diffusion impedance increased with the increasing oxygen content, which was related to the H_2O and CO_2 in the reaction products that were unfavorable to the electrochemical reaction of the anode.

Table 4. Output performance of the cells under various CH_4/O_2 gas mixtures

CH_4-O_2-Ar (sccm)	R_{in}	OCV (V)	MPD (mW/cm^2)	R_{ohm} (Ω cm^2)
50-10-50	5	1.09	428	0.126
50-20-50	2.5	1.08	467	0.120
50-30-50	1.67	1.07	497	0.137
50-40-50	1.25	1.02	419	0.142
50-50-50	1	0.98	360	0.147

The major issue for the active electrodes is their stability during long-term operation at the working temperature. The cell voltage at R_{in} = 2.5 was stable at 0.9 V with a current density of 100 mA/cm^2, as shown in Fig. 8. Oscillation was not observed during the test. Zhang et al. [28-29] reported that the oscillatory behaviors during the partial oxidation of methane could be affected by the feed gas composition. Napporn and co-workers [30] showed a performance degradation with OCV oscillation due to the redox reaction of Ni in oxygen-rich gas mixtures. Kellogg et al. [31] also believed that the oscillatory behavior was caused by the redox reaction that occurred on the Ni-anode. According to our measurements under the different operating conditions and all the property characterizations, R_{in} = 2.5 was determined to provide the outcomes of interest for SOFC operation optimization. A basic equilibrium of Ni oxidation and NiO reduction occurred at R_{in} = 2.5. Ni did not lose its catalytic activity and the partial oxidation of methane continued to provide H_2 and CO for the anode, which made the cell stable.

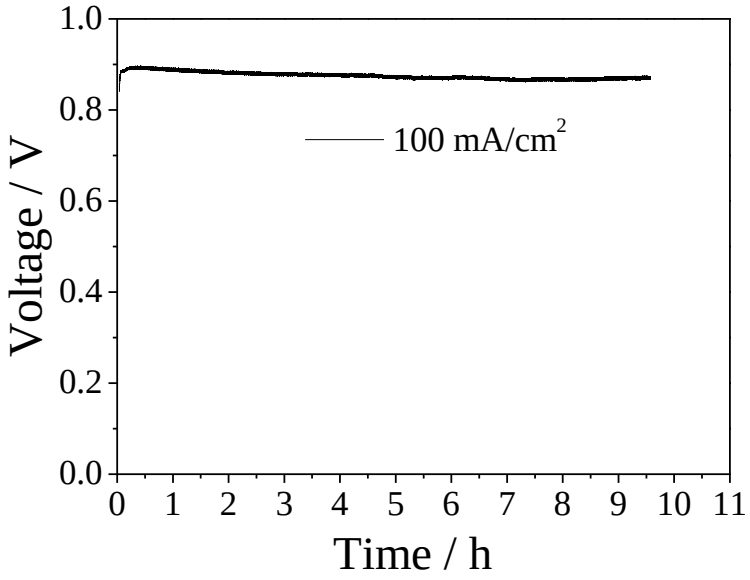

Figure 8. Voltage-time curve at a current density of 100 mA/cm^2 at 700 °C

Table 5. Materials and gas components for methane oxidation reported in the literature

Materials	Gas components	Total flow rate	Performance characterization	Test conditions	Reference
$Ni/Ce_{0.90}Y_{0.10}O_{1.950}$	CH_4:O_2:Ar = 2:1:3	GHSV of 36000 ml/g/h	CH_4 conversion of 78.8%	850 °C	1
$Ni/Gd_{0.2}Ce_{0.8}O_{1.9-\delta}$	CH_4:O_2 = 2:1	120 sccm	SOFC with power density of 1.35 W/cm^2, stable operated over 500 h	650 °C	15
$La_{0.08}Sr_{0.92}Fe_{0.20}Ti_{0.80}O_{3-\delta}$	CH_4:O_2 = 2:1 in Ar	50 sccm	CH_4 conversion of 52%	900 °C	32
$NiO/Ce_{0.75}Zr_{0.25}O_2$	CH_4:O_2 = 2:1	100 sccm	CH_4 conversion of 80%	800 °C	33
Ni/CeO_2	CH_4:O_2 = 2:1 in He	50 sccm	CH_4 conversion of 98%	700-800 °C	34
Ni/YSZ	CH_4:air = 3:1	40 sccm	SOFC stability improved by suppressing coking in Ni anodes	800 °C	13
Ni/YSZ	CH_4:air = 5:1	600 sccm	Both carbon deposition and anode layers delamination were avoided	800 °C	14

Until recently, most of the studies of the catalytic oxidation of methane in SOFCs were focused on the methane-to-oxygen ratio of 2, which is the stoichiometric value for the partial oxidation of methane. Table 5 lists the anode materials and gas components reported in the literature. Few papers considered the effect of adding air to methane on the methane oxidation behavior. According to Aslannejad et al. [14], the anodic feeding compositions of the methane (500 sccm) dilution with air flow

rates of 50-800 sccm were explored for Ni/YSZ anode supported cells at 800 °C. Experimental results showed that 1:5 air to methane addition was the optimal gas composition. Both carbon deposition and anode delamination were avoided. A stable cell operation at 0.6 V was guaranteed. Gong et al. [35] demonstrated a SOFC module coupled with a catalytic partial oxidation reformer with Rh supported by Al_2O_3 as the catalyst. Methane and air gas mixtures of 40 sccm were applied to evaluate the performance of the reformer with various C/O ratios. The optimal C/O ratio of 0.8 was obtained at 800 °C with a maximum reforming efficiency of 86.1%. Based on our findings, the methane addition with oxygen carriers with a ratio of 2.5 was found to be a good solution to restrain carbon deposition and Ni oxidation for the Ni/YSZ anodes.

4. CONCLUSION

This paper studied the catalytic activity of methane oxidation over Ni/YSZ anodes fueled under various methane-oxygen mixtures. The following conclusions can be drawn. The catalytic activity tests of Ni/YSZ catalyst indicated that the complete oxidation reaction of methane was the dominant reaction at $R_{in} = 1$, and the reaction at $R_{in} \geq 1.25$ was dominated by the partial methane oxidation. Catalytic reforming reactions of methane at 700 °C showed that Ni oxidation occurred at $R_{in} \leq 1.67$. Through experimental activity under different operating conditions and suitable performance characterizations, $R_{in} = 2.5$ was determined to exhibit the best activity among the Ni/YSZ electrodes.

ACKNOWLEDGEMENT
This work was supported by the National Natural Science Foundation of China (Nos. 51602213, 11604236 and 61575139) and the Youth Foundation of the Taiyuan University of Technology (No. 2015QN071).

References

1. S.H. Zeng, L. Wang, M.C. Gong and Y.Q. Chen, *J. Nat. Gas Chem.*, 19 (2010**)** 509.
2. J.W. Yun, S.P. Yoon, H.S. Kim, J. Han and S.W. Nam, *Int. J. Hydrogen Energy*, 37 (2012) 4356.
3. J.H. Koh, Y.S. Yoo, J.W. Park and H.C. Lim, *Solid State Ionics*, 149 (2002) 157.
4. K. Kendall, C.M. Finnerty, G. Saunders and J.T. Chung, *J. Power Sources*, 106 (2002) 323.
5. W. Wang, C. Su, Y. Wu, R. Ran and Z. Shao, *Chem. Rev.*, 113 (2013) 8104.
6. A. Gunji, C. Wen, J. Otomo, T. Kobayashi, K. Ukai and Y. Mizutani, *J. Power Sources*, 131 (2004) 285.
7. R.J. Gorte and J.M. Vohs, *J. Catal.*, 216 (2003) 477.
8. S. Mclntosh and R.J. Gorte, *Chem. Rev.*, 104 (2004) 4845.
9. B.S. Barros, D.M.A. Melo, S. Libs and A. Kiennemann, *Appl. Catal. A-Gen.*, 378 (2010) 69.
10. M.R. Cesário, B.S. Barros, C. Courson, D.M.A. Melo and A. Kiennemann, *Fuel Process Technol.*, 131 (2015), 247.
11. Y. Wang, X. Hong, B. Li, W. Wang and D. Wang, *J. Nat. Gas Chem.*, 17 (2008) 344.
12. G.J. Offer, J. Mermelstein, E. Brightman and N.P. Brandonz, *J. Am. Ceram. Soc.*, 92 (2009) 763.
13. M. Pillai, Y. Lin, H. Zhu, R.J. Kee and S.A. Barnett, *J. Power Sources*, 195 (2010) 271.
14. H. Aslannejad, L. Barelli, A. Babaie and S. Bozorgmehri, *Applied Energy*, 177 (2016) 179.

15. D. Lee, J. Myung, J. Tan, S-H. Hyun, J. TS. Irvine, J. Kim and J. Moon, *J. Power Sources*, 345 (2017) 30.
16. X. Jacques-Bedard, T.W. Napporn, R. Roberge and M. Meunier, *J. Electrochem. Soc.*, 154 (2007) B305.
17. Z. Wang, Z. Lü, B. Wei, K. Chen, X. Huang, W. Pan and W. Su, *Electrochim. Acta*, 56 (2011) 6688.
18. K.F. Chen, Z. Lu, N. Ai, X.Q. Huang, Y.H. Zhang, X.S. Xin, R.B. Zhu and W.H. Su, *J. Power Sources*, 160 (2006) 436.
19. B. Wei, Z. Lu, X.Q. Huang, M.L. Liu, K.F. Chen and W.H. Su, *J. Power Sources*, 167 (2007) 58.
20. J. Macek, B. Novosel and M. Marinsek, *J. Eur. Ceram. Soc.*, 27 (2007) 487.
21. C.M. Finnerty, N.J. Coe, R.H. Cunningham and R.M. Ormerod, *Catal. Today*, 46 (1998) 137.
22. I. Riess, *J. Power Sources*, 175 (2008) 325.
23. M. Kuhn and T.W. Napporn, *Energies*, 3 (2010) 57.
24. S. Savoie, T.W. Napporn, B. Morel, M. Meunier and R. Roberge, *J. Power Sources*, 196 (2011) 3713.
25. V.Y. Bychkov, V.P. Tyulenin, V.N. Korchak and E.L. Aptekar, *Appl. Catal. A-Gen.*, 304 (2006) 21.
26. T. Suzuki, P. Jasinski, V. Petrovsky, H.U. Anderson and F. Dogan, *J. Electrochem. Soc.*, 151 (2004) A1473.
27. B. Morel, R. Roberge, S. Savoie, T. Napporn and M. Meunier, *Appl. Catal. A-Gen.*, 323 (2007) 181.
28. X.L. Zhang, D.O. Hayward and D.M.P. Mingos, *Catal. Lett.*, 86 (2003) 235.
29. X.L. Zhang, C.S.M. Lee, D.O. Hayward and D.M.P. Mingos, *Catal. Today*, 105 (2005) 283.
30. X. Jacques-Bedard, T.W. Napporn, R. Roberge and M. Meunier, *J. Power Sources*, 153 (2006) 108.
31. I.D. Kellogg, U.O. Koylu, V. Petrovsky and F. Dogan, *Int. J. Hydrogen Energy*, 34 (2009) 5138.
32. J.S. Yoon, E.J. Yi, B.H. Choi, M-J. Ji and H. J. Hwang, *Ceram. Int.*, 40 (2014) 1525.
33. V.R. da Silveira, D.M.A. Melo, B.S. Barros, J.A.C. Ruiz and L.O.A. Rojas, *Ceram. Int.*, 42 (2016) 16084.
34. G. Pantaleo, V. La Parola, F. Deganello, R.K. Singha, R. Bal and A.M. Venezia, *Appl. Catal. B-Environ.*, 189 (2016) 233.
35. S.Q. Gong, H.Y. Zeng, J. Lin, Y.X. Shi, Q. Hu and N.S. Cai, *J. Power Sources*, 402 (2018) 124.